Euro. Jnl of Applied Mathematics (2012), *vol.* 23, *pp.* 315–341.
doi:10.1017/S0956792511000398

Characterising the disordered state of block copolymers: Bifurcations of localised states and self-replication dynamics

KARL B. GLASNER

Department of Mathematics and Program in Applied Mathematics, University of Arizona, Tucson, AZ 85721, USA4
email : kglasner@math.arizona.edu

(*Received 10 March 2011; revised 8 November 2011; accepted 9 November 2011; first published online 21 December 2011*)

Above the spinodal temperature for micro-phase separation in block co-polymers, asymmetric mixtures can exhibit random heterogeneous structure. This behaviour is similar to the sub-critical regime of many pattern-forming models. In particular, there is a rich set of localised patterns and associated dynamics. This paper clarifies the nature of the bifurcation diagram of localised solutions in a density functional model of $A-B$ diblock mixtures. The existence of saddle-node bifurcations is described, which explains both the threshold for heterogeneous disordered behaviour as well the onset of pattern propagation. A procedure to generate more complex equilibria by attaching individual structures leads to an interwoven set of solution curves. This results in a global description of the bifurcation diagram from which dynamics, in particular self-replication behaviour, can be explained.

Key words: Co-polymer; Order–disorder transition; Self-replication

1 Introduction

Block co-polymers are macromolecules built from two or more monomer sub-chains. At low enough temperatures (typically characterised by large χN, the familiar interaction parameter), micro-phase segregation occurs and a wide array of micro-structures can be created [3, 16, 18, 26].

The simplest situation is the AB diblock made up of monomers A and B. These are observed to form a variety of mesophases such as body-centred cubic, hexagonal, lamellar and other bicontinuous structures [27]. These phases are generally regarded as spatially periodic, global energy minimisers [3], although in practice they are not readily observed without considerable intervention [2]. This difficulty has been ascribed to kinetic trapping of local minima of the free energy [47].

At temperatures above the region for mesophase formation, the mixture is not necessarily homogeneous. Physical experiments have identified a variety of structured states without long-range order [19, 34, 38, 39, 44]. The most conspicuous manifestation of these are randomly distributed spherical micelles [39, 44], which gradually increase in concentration as the ordered regime is approached.

The transition from the disordered state to the ordered one has been actively investigated over the past decade. The concentration of disordered micelles as a function of temperature was first predicted theoretically by Dormidontova and Lodge [13]. They modelled micelles using Seminov's strong segregation theory [40], and assumed thermodynamic equilibrium between micellised and un-micellised polymers. Wang *et al.* [43] regard the appearance of micelles as a (thermally) activated process, and use self-consistent field theory calculations to find the shape of localised concentration fluctuations.

Micelles and other non-periodic structures can be investigated theoretically as localised, steady state patterns of the underlying model. This approach was taken by Glasner [17], who identified localised one-, two-, and three-dimensional equilibria in a density functional model, as well as some of their associated dynamics. Similar to the mean-field model results of Wang *et al.* [43], there is a critical value of parameter $\chi N = (\chi N)_{MD}$ below which no localised solutions exist (they call this the micelle dissociation temperature). It was observed that there is a larger value $(\chi N)_{SR}$, smaller than the spinodal value $(\chi N)_s$, above which localised solutions give way to pattern propagation which ultimately fills the domain. In the interval $(\chi N)_{MD} \leqslant \chi N \leqslant (\chi N)_{SR}$, there is a multiplicity of stable and unstable solution branches describing clustered arrangements, which are one focus of the present work.

The interwoven bifurcation diagram which emerges is similar to many other pattern forming systems which exhibit subcritical bifurcations (that is, in a regime where the base state is linearly stable) [10]. There have been two recent, complementary explanations of this situation, commonly referred to as 'homoclinic snaking' by virtue of the shape of the bifurcation curves. Chapman and Kozyreff [7] take a multiple scales approach, looking for localised steady states of the sub-critical Swift–Hohenberg equation

$$u_t = -ru - \left(1 + \partial_x^2\right)^2 u + Au^2 + Bu^3, \quad r > 0,$$

by computing exponentially small terms that arise in the expansion. The compatibility of these small terms gives rise to algebraic criteria that allow the construction of a bifurcation diagram. In contrast, Beck *et al.* [4] take a qualitative geometric viewpoint. They regard localised states as homoclinic orbits of a map arising from the steady state ordinary differential equations (ODEs). The complex snaking bifurcation picture emerges from the interwoven tangle of stable and unstable manifolds.

In contrast to wave-packet-type solutions explored in [7], the structures we describe more closely resemble peaks (sometimes called spikes or spots). Figure 5 shows examples of localised steady states for the present model. Small-amplitude solutions near $(\chi N)_s$ are in fact described by oscillations with slow modulation. But as the bifurcation diagram is traversed, certain oscillations become pronounced, and distinct peaks form.

There are also dynamical phenomena related to the intricate bifurcation of localised states. In the region just below the point of instability (spinodal decomposition here), pattern propagation is commonly observed. In the present case, this takes the form of self-replication (e.g. [12, 23, 30, 35, 37]) of individual structures. Nishiura and Ueyama [30] proposed a general theory for this behaviour, based upon the simultaneous disappearance via saddle-node events of all solution branches as the bifurcation diagram is traversed.

https://doi.org/10.1017/S0956792511000398 Published online by Cambridge University Press

The dynamical after-effect is a transition to patterns with a greater and greater number of fundamental units.

Although localised states are commonly associated with self-replication dynamics, there is very little literature that marries these two topics. This work serves as both a case study that shows how these ideas interrelate as well as a clarification of the bifurcation diagram particularly to block co-polymer mixtures.

The paper is organised as follows. A fundamental branch of localised states is first identified, and characterised in terms of the asymptotic scaling on different parts of the branch. More complex equilibria can be built upon this fundamental structure, leading to a robust qualitative picture of merging and bifurcations of various solution branches. From this, one ascertains the heteroclinic connections that form a basis for dynamical behaviour. This ultimately explains the emergence of self-replication behaviour that precedes spinodal decomposition.

2 The density functional model

The model employed here is a version of the standard Ohta & Kawasaki [31] free energy density functional

$$F(\phi) = \int \frac{a}{2}|\nabla\phi|^2 + g(\phi;\chi N)dx + \frac{\gamma}{2}\iint G(x-x')[\phi(x)-f][\phi(x')-f]\,dx\,dx'. \qquad (2.1)$$

Here, ϕ is the volume fraction of A monomers (where by the standard incompressibility assumption $1-\phi$ is the B-monomer density), G is the usual free-space Green's function for the Laplacian, and g is a double-well energy. As with self-consistent mean-field theories [20, 21, 24, 27], there are two dimensionless parameters: χN, representing the Flory–Huggins-type interaction energy between monomers, and the mean volume fraction f of A-monomers.

There are a variety of ways to specify the potential and coefficients [5, 8, 32, 41] either based on first principles or invoking some empirical criteria. The specific form used here is a compromise between these two aims and was described in detail in [17]. The idea is to reproduce the linear (spinodal) instability in a controlled way and calibrate the diffuse interface thickness. This can be accomplished with a potential of the form

$$g(\phi) = h(\phi) + \chi N\phi(1-\phi), \qquad (2.2)$$

where the convex part h is calibrated to match Leibler's well-known theory based on the random phase approximation [24] at linear order. A good fit suitable to numerical and analytical solution was found to be [17]

$$h \approx -a_1(\ln(\phi) + \ln(1-\phi)) + a_2\phi(1-\phi) + a_3\phi^2(1-\phi)^2, \qquad (2.3)$$

where $a_1 = 1.3, a_2 = 0.23, a_3 = 6.05$. The other parameters in equation (2.1) were determined to be $a \approx 2.3$ and $\gamma = \gamma(f) = q^*(f)^4$, where q^* is the most unstable wavenumber at the spinodal point. Reasonable quantitative agreement between this model and a mean-field approach [43] was found for isolated micelle-type solutions in our previous work [17]. It

https://doi.org/10.1017/S0956792511000398 Published online by Cambridge University Press

should be emphasised that the particular forms, that is equations (2.2) and (2.3), are given for specificity, but have little influence on the qualitative results of this paper.

A dynamical model is employed here which follows the standard viewpoint of diffusive transport arising from gradients of the chemical potential $\delta F/\delta\phi$ [29]. This can be equivalently characterised as a Cahn–Hilliard-type gradient flow, leading to

$$\phi_t = \Delta\left[\frac{\delta F}{\delta\phi}\right] = -a\Delta^2\phi + \Delta g_\phi(\phi;\chi N) + \gamma(f-\phi). \tag{2.4}$$

where the scale for t has been chosen to absorb the diffusion coefficient. Note that the mean volume constraint on a domain V

$$\int_V (\phi - f)dx = 0, \tag{2.5}$$

is automatically enforced for time-independent solutions of equation (2.4) with suitable no-flux boundary conditions.

3 Localised solutions in one dimension

Many pattern-forming systems exhibit a sub-critical bifurcation that leads to steady states which are localised, that is, they decay exponentially in the far field. In the context of block co-polymers, these are bilayer- or micelle-type architectures that exist within a stable homogeneous mixture. In contrast to standard amphiphiles, there is no solvent that prefers one of the co-polymer components; these structures exist simply because of the energetic advantage of phase separation.

One-dimensional steady states $\phi(x)$ in our problem are homoclinic orbits of the underlying ODE

$$-a\phi_{xxxx} + (g_\phi(\phi;\chi N))_{xx} + \gamma(f-\phi) = 0, \quad \phi - f = \mathcal{O}(-\exp(|x|/\lambda)), \quad |x| \to \infty, \tag{3.1}$$

where λ denotes some undetermined decay length-scale. Solutions to this problem were previously investigated in [17], and those results are summarised below.

Linearisation of the dynamic equation about $\phi = f$ gives the spinodal point (technically a curve in two-dimensional parameter space), where the linearised growth rate $\sigma(k) = -ak^4 - g''(f;\chi N)k^2 - \gamma$ is marginal, specifically

$$(\chi N)_s = \frac{h''(f) + \sqrt{4a\gamma}}{2}. \tag{3.2}$$

Linearisation of the steady state equations gives the far-field behaviour, and is related to the linearised dynamics. For $\chi N > (\chi N)_s$, there cannot be any decay and therefore no localised states exist. For $\chi N < (\chi N)_{osc}$, where $\chi N_{osc} = h''(f)/2$, the tails of localised solutions must be strictly exponential. For $(\chi N)_{osc} < \chi N < (\chi N)_s$, the tails oscillate with ever decreasing spatial decay as the spinodal value is approached.

Localised solutions describing single peaks in density were investigated numerically [17], and the results are reproduced in Figure 1. The lower boundary for existence is $\chi N = (\chi)_{MD}(f)$ (the 'micelle disassociation' temperature), which can be either less or greater

https://doi.org/10.1017/S0956792511000398 Published online by Cambridge University Press

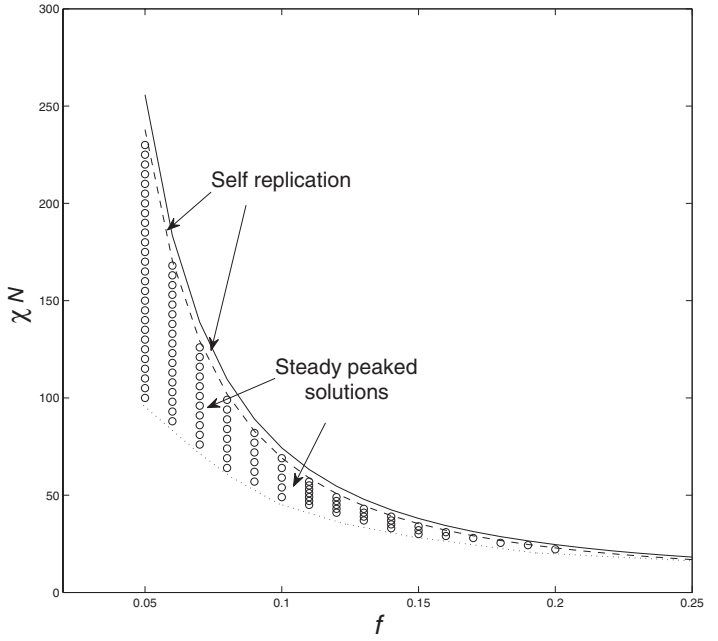

FIGURE 1. Phase diagram for one-dimensional steady solutions (the domain is regarded as infinite). The solid line is the spinodal curve, above which the homogeneous state is unstable. The region between the dotted ($(\chi N)_{MD}$) and dashed line ($(\chi N)_{SR}$) is where steady solutions were found, represented by circles. Between the solid and dashed line, self-replicating behaviour is observed. For $f > 0.3$, no solutions were found (see Section 3.2).

than $(\chi N)_{osc}$. The upper boundary $\chi N = (\chi N)_{SR}(f)$ is always in the interval $[(\chi N)_{osc}\ (\chi N)_s]$. The other salient aspect is the existence of a maximum value of composition fraction $f = f_{max}$, above which steady solutions (in A-monomer density) do not exist at all. (By virtue of symmetry of the model, one has an equivalent picture for localised concentrations of B-monomer density). The purpose of this section is to clarify where and why all of these bifurcation points exist.

3.1 Existence and stability of localised states

Some general observations about solutions to equation (3.1) are useful. On one hand, this equation captures critical points of equation (2.1) since it is the (twice differentiated) Euler–Lagrange equation. One can view it differently, however, by considering just the convex part of (2.1)

$$F_c(\phi) = \int_{-\infty}^{\infty} \frac{a}{2}\phi_x^2 + h(\phi)dx + \frac{\gamma}{2}\iint G(x-x')[\phi(x)-f][\phi(x')-f]\,dx\,dx', \tag{3.3}$$

and the (nonlinear) constraint

$$\int_{-\infty}^{\infty} (\phi - f)^2 dx = L \tag{3.4}$$

https://doi.org/10.1017/S0956792511000398 Published online by Cambridge University Press

(unless specified, integration will always be over the real line). It is straightforward to see that finding critical points of equation (3.3) subject to equation (3.4) leads to

$$\frac{\delta F_c}{\delta \phi} = \Lambda(\phi - f), \tag{3.5}$$

where Λ is a Lagrange multiplier. Differentiating twice, one discovers that this equation is the same as equation (3.1), with $2\chi N$ playing the role of the Lagrange multiplier.

For each L, one can attempt to find a constrained minimiser. Since equation (3.3) is bounded from below, there is a minimising sequence ϕ_n such that $F_c(\phi_n)$ is decreasing and limits to the infimum. If the domain was finite, one can use standard compactness arguments [15] to construct a minimiser. For an infinite domain, the minimising sequence could either tend toward a non-trivial function, or could have a (weak) limit which is simply the base state $\phi \equiv f$. The distinction between the two cases will be made clear in the next section by identifying the cross-over between small-amplitude and zero-amplitude steady states. In the former case, there exists a nontrivial branch of solutions of equation (3.1), given as $\phi(x; L), \chi N(L)$ (see Figure 5 for a numerical study). Note that in assuming decay of ϕ, $\chi N(L) < (\chi N)_s$.

The bifurcation diagram is naturally related to the stability of branches. One expects that there is a switching of sign of an eigenvalue at fold points, for example. This leads to the conclusion that there must exist an unstable solution branch near fold points (see, e.g. Maddocks [25]).

The idea to regard stationary solutions as constrained minimisers has even more implications. Stability of the solutions $\phi(x; L)$ is equivalent to positivity of the bilinear form associated with the second variation

$$B(\psi, \psi) = \int \psi \mathscr{L}_{\phi(L)} \psi \, dx, \tag{3.6}$$

where

$$\mathscr{L}_{\phi(L)} \equiv \frac{\delta^2 F(\phi(L)}{\delta \phi^2} \equiv \mathscr{L}^c_{\phi(L)} - 2\chi N, \tag{3.7}$$

and integration is over the whole domain. Consider the specific test function $\psi = d\phi_L/dL$. We can write

$$B(\psi, \psi) = \int \left[\mathscr{L}^c_{\phi(L)} \frac{d\phi(L)}{dL} - \Lambda(L) \frac{d\phi(L)}{dL} \right] \frac{d\phi(L)}{dL} \, dx, \tag{3.8}$$

where $\Lambda(L) = 2\chi N(L)$ is the associated Lagrange multiplier satisfying equation (3.5). Assuming that $\phi(L)$ describes a continuously differentiable branch of solutions, differentiating equations (3.4) and (3.5) with respect to L gives

$$\int \frac{d\phi(L)}{dL}(\phi(L) - f) \, dx = \frac{1}{2}, \quad \int \mathscr{L}^c_{\phi(L)} \frac{d\phi(L)}{dL} \, dx = \frac{d\Lambda(L)}{dL}(\phi(L) - f) + \Lambda \frac{d\phi(L)}{dL}. \tag{3.9}$$

Combining with (3.8), it follows that

$$B(\psi, \psi) = \frac{d\Lambda}{dL} \int \frac{d\phi(L)}{dL}(\phi(L) - f) = \frac{1}{2} \frac{d\Lambda}{dL}. \tag{3.10}$$

https://doi.org/10.1017/S0956792511000398 Published online by Cambridge University Press

If $d\chi N(L)/dL < 0$ (which is necessarily true for solutions immediately bifurcating from the flat state), the second variation is non-positive and the solutions are unstable.

Demonstrating stability is somewhat more delicate. First, let us verify the following: if $\phi(L)$ is a constrained local minimiser of F_c, then $\mathscr{L}_{\phi(L)}$ can only have at most one unstable eigenvalue. Supposing the opposite were true, there would exist orthogonal eigenfunctions ψ_1, ψ_2 such that

$$\mathscr{L}_{\phi(L)}\psi_{1,2} = \lambda_{1,2}\psi_{1,2}, \quad \lambda_{1,2} < 0. \tag{3.11}$$

We can form a superposition $\psi_\epsilon = \epsilon(a_\epsilon\psi_1 + b_\epsilon\psi_2)$ so that $\phi(L) + \psi_\epsilon$ exactly satisfies the constraint (3.4), and so that a_ϵ, b_ϵ limit to constants bounded away from zero as $\epsilon \to 0$. Notice that F and F_c coincide (up to a constant) on the constraint surface (3.4), therefore

$$F(\phi(L) + \psi_\epsilon) - F(\phi(L)) = F_c(\phi(L) + \psi_\epsilon) - F_c(\phi(L)) \geqslant 0. \tag{3.12}$$

On the other hand,

$$\begin{aligned} F(\phi(L) + \psi_\epsilon) - F(\phi(L)) &= B(\psi_\epsilon, \psi_\epsilon) + \int \Big[h(\phi(L) + \psi_\epsilon) \\ &\quad - h(\phi(L)) - h'(\phi(L))\psi_\epsilon - \frac{1}{2}h''(\phi(L))\psi_\epsilon^2\Big]dx \\ &\equiv \epsilon^2\big(a_\epsilon^2\lambda_1 + b_\epsilon^2\lambda_2\big) + R_\epsilon. \end{aligned} \tag{3.13}$$

Note that the integrand in R_ϵ is just the remainder of the Taylor expansion to two orders, and therefore can be estimated as

$$R_\epsilon \leqslant C\epsilon^3 \int \big(a_\epsilon^2\lambda_1 + b_\epsilon^2\lambda_2\big)^3 dx, \tag{3.14}$$

where C is some constant independent of ϵ. The integral in this expression is bounded since it can be shown that the eigenfunctions $\psi_{1,2}$ decay exponentially at infinity. Thus, $R = \mathcal{O}(\epsilon^3)$ so that for small enough ϵ, $F(\phi(L) + \psi_\epsilon) - F(\phi(L)) < 0$, which contradicts equation (3.12).

It follows that if the solution curve $\phi(L)$ has a saddle-node (fold) bifurcation where $d\chi N(L)/dL$ switches sign, it must involve a switching of the sign of the single potentially unstable eigenvalue of $\mathscr{L}_{\phi(L)}$. That is, one branch must be stable and the other unstable. We call the combination of lowest amplitude (smallest L) stable and unstable solutions as the *fundamental* branch.

In the remainder of this section, solutions are examined in more detail by considering various limiting cases. Each subsection corresponds to a particular part of the fundamental branch as shown in Figure 2.

3.2 Small-amplitude solutions and the Maxwell point

Near the spinodal point, one expects bifurcation from the flat state $\phi = f$. To this end, it is useful to look for multiple-scale solutions whose envelope amplitude is small and varies slowly in space with respect to the underlying marginally stable wavelength. This expansion serves as a starting point to identify the fundamental branch of solutions which

https://doi.org/10.1017/S0956792511000398 Published online by Cambridge University Press

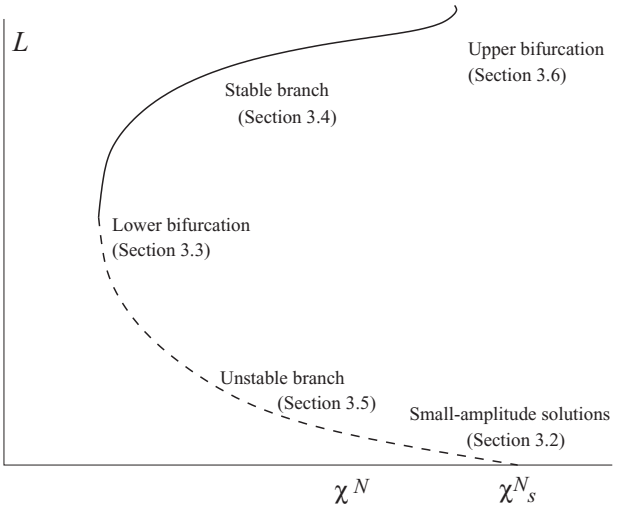

FIGURE 2. Correspondence between different parts of the fundamental solution branch and subsections which analyse each region as a limiting case.

can be continued to larger amplitude. Other small-amplitude solutions exist as a matter of gluing these fundamental units together which is pursued later. The important quantitative result of this section is to identify the region in parameter space where the subcritical bifurcation point vanishes. This is conventionally known as the Maxwell point [36] by analogy to the co-existence point of phase transitions. For this purpose, it is sufficient to study small-amplitude solutions. We use a multiple-scale ansatz similar to Budd *et al.* [6].

By setting $u = \phi - f$ and rescaling $X = (\gamma/a)^{1/4}$, equation (3.1) can be rewritten as

$$\mathscr{L}_\epsilon u = -(H(u))_{XX}, \quad \mathscr{L}_\epsilon \equiv -\frac{d^4}{dX^4} + (\epsilon - 2)\frac{d^2}{dX^2} - 1, \tag{3.15}$$

where

$$\epsilon \equiv \frac{2((\chi N)_s - \chi N)}{\sqrt{a\gamma}}, \tag{3.16}$$

and H is the nonlinear part of h':

$$H(u) = \frac{h'(f+u) - h''(f)u}{\sqrt{a\gamma}}. \tag{3.17}$$

By expanding

$$u = \epsilon^{\frac{1}{2}} U_1(x, y) + \epsilon U_2(x, y) + \epsilon^{\frac{3}{2}} U_3(x, y) + \cdots, \quad y \equiv \epsilon^{\frac{1}{2}} x, \tag{3.18}$$

at leading order, one gets $\mathscr{L}_0 U_1 = 0$, which has the even-symmetry solution

$$U_1 = A(y)\cos(x). \tag{3.19}$$

https://doi.org/10.1017/S0956792511000398 Published online by Cambridge University Press

The next order in the expansion reads (regarding derivatives in $\mathscr{L}$ as acting on x)

$$\mathscr{L}_0 U_2 = -\frac{1}{2}H''(0)(U_1^2)_{xx} = H''(0)A^2(y)\cos(2x), \tag{3.20}$$

leading to the particular solution

$$U_2^p = -\frac{1}{9}h'''(0)A^2(y)\cos(2x). \tag{3.21}$$

The complete solution is therefore $U_2 = A_2(y)\cos(x) + B_2(y)\sin(x) + U_2^p$.

At the next order, one has

$$\begin{aligned}\mathscr{L}_0 U_3 - 4(U_2)_{xxxy} - 6(U_1)_{xxyy} + 2(U_1)_{yy} + (U_1)_{xx} - 4(U_2)_{xy} \\ = -H''(0)(U_1U_2)_{xx} - \frac{1}{6}H'''(0)(U_1^3)_{xx} - H''(0)(U_1^2)_{xy}.\end{aligned} \tag{3.22}$$

The balance of remaining secular terms (i.e. those in the nullspace of $\mathscr{L}_0$) gives the amplitude equation

$$4A'' - A + \beta A^3 = 0, \quad \beta = \frac{1}{18}H''(0)^2 - \frac{1}{8}H'''(0). \tag{3.23}$$

This system is Hamiltonian, and there are two cases to consider. If $\beta > 0$, then there exist two homoclinic orbits connecting the origin. The positive homoclinic branch $A > 0$ can be continued to large amplitudes, giving a single-peak profile; in contrast, the negative branch grows to a two-peak even symmetry solution. If $\beta < 0$, no homoclinic orbits exist. The "Maxwell point' can be determined by setting $\beta = 0$ in equation (3.23), which gives a relationship between f and other problem parameters. Using the calibrated potential (2.3), this implies that there are no localised solutions when the volume fraction $f \gtrsim 0.3$. This is more or less in accord with numerical results [17].

3.3 The lower bifurcation point

The remainder of this section concentrates on the limit of small f in order to ascertain the nature of bifurcations quantitatively. Throughout, we exploit the scaling $\gamma \sim f^{-1}$ which comes from the underlying calibration of the model described in [17]. This leads, via dominant balance, to natural choices for the scaling of other quantities.

To capture the structure of solutions near the lower bifurcation point $(\chi N)_{MD}$, we suppose that $\chi N \sim f^{-1}$. There are three regions with different scales for ϕ and x: an interior region of width $\mathcal{O}(f^{1/2})$, a narrow transition layer of width $\mathcal{O}(f)$, and an outer region of width $\mathcal{O}(f^{-1/2})$. To avoid superfluous notation, the variable ϕ will generally be left unscaled, and its solution in different regions will be obvious from the independent variable employed.

For the first region described above, set $x = zf^{1/2}$. Leading order balance gives

$$-a\phi_{zzzz} - 2f(\chi N)\phi_{zz} = 0. \tag{3.24}$$

https://doi.org/10.1017/S0956792511000398 Published online by Cambridge University Press

By virtue of matching to the intermediate region on the right (where $\phi = \mathcal{O}(f)$) and symmetry, this integrates to

$$\phi = A\left[\cos\left(\sqrt{\frac{2f\chi N}{a}}z\right) + 1\right], \quad 0 < z < z_f, \quad z_f \equiv \pi\sqrt{\frac{a}{2f\chi N}}, \tag{3.25}$$

where A is as yet undetermined.

The second region is a wide outer region where $\phi \sim f$ and a re-scaled coordinate Z is defined by $x = Zf^{-1/2}$. The leading order problem is now

$$-fa_1\left(\frac{1}{\phi}\right)_{ZZ} + \gamma(f - \phi) = 0. \tag{3.26}$$

Letting $w = 1/\phi$, one can integrate the resulting equation using $\lim_{Z\to\infty} w = 1/f$, giving

$$\frac{fa_1}{2}w_Z^2 + \gamma\left(\ln(fw) - fw + 1\right) = 0. \tag{3.27}$$

The complete solution by further integration requires the undetermined matching value

$$\phi^* \equiv \lim_{Z\to 0}\phi(Z) = \lim_{Z\to 0}\frac{1}{w(Z)}.$$

The third region is between the inner and outer regions and uses the re-scaled coordinate $\zeta = f^{-1}(x - z_f f^{1/2})$. To be consistent with matching to the outer region, one needs $\phi = O(f)$. At leading order,

$$-a\phi_{\zeta\zeta\zeta\zeta} - a_1 f^2\left(\frac{1}{\phi}\right)_{\zeta\zeta} = 0. \tag{3.28}$$

Integrating twice and matching to the outer region gives

$$-a\phi_{\zeta\zeta} - a_1 f^2\left(\frac{1}{\phi} - \frac{1}{\phi^*}\right) = 0. \tag{3.29}$$

Integrating this and matching to the first inner region connects the undetermined constants A and ϕ^*:

$$\phi_{zz}(z = \pi\sqrt{a/2f(\chi N)}) = \frac{2Af\chi N}{a} = \frac{1}{f^2}\lim_{\zeta\to-\infty}\phi_{\zeta\zeta} = \frac{a_1}{a\phi^*}. \tag{3.30}$$

The final ingredient that determines the solution is a Fredholm-type solvability across all three regions. By virtue of the fact that the linearisation of equation (3.1) about any leading order solution yields an adjoint operator with unity in its nullspace, one discovers that this solvability condition is nothing more than the volume fraction constraint (2.5) at leading order. This means that the volume fraction surplus in the inner region must balance the deficit in the outer region; in scaled variables, this reads

$$\int_0^{\pi\sqrt{\frac{a}{2f\chi N}}}\phi(z)dz = \frac{1}{f}\int_0^{\infty}(f - \phi(\zeta))d\zeta,$$

which can be computed from equations (3.25) and (3.27). This provides a second algebraic

https://doi.org/10.1017/S0956792511000398 Published online by Cambridge University Press

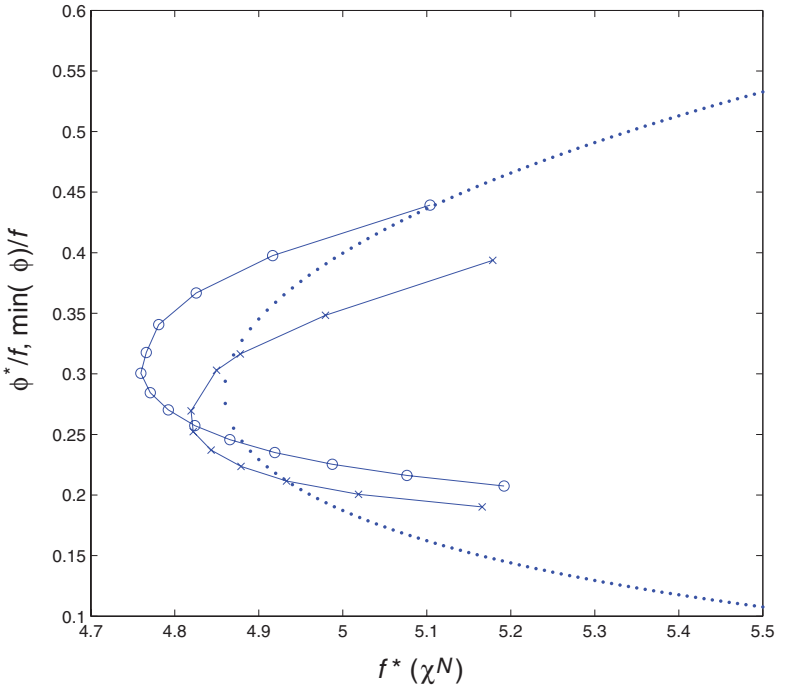

FIGURE 3. (Colour online) Solution to equation (3.31) (shown as dotted line) compared to numerical solutions of steady states for $f = 0.1$ (circles) and $f = 0.05$ (x's). The vertical axis is the value ϕ^* (for asymptotics) or the minimum value of ϕ for a single-peak solution (for numerical solutions). Note the axes are scaled according to the presumed dependence on f.

relationship between A and ϕ^*, from which one can eliminate A in equation (3.30) to arrive at

$$\frac{a_1\pi\sqrt{a}}{\phi^*(2\chi N)^{3/2}} = \sqrt{\frac{2a_1}{\gamma}\left(f/\phi^* - \ln(f/\phi^*) - 1\right)}. \tag{3.31}$$

This algebraic equation for ϕ^* yields a saddle-node bifurcation in the parameter χN (see Figure 3). Consequently, there are two branches of solutions which form as χN is increased: a larger amplitude branch (corresponding to lower ϕ^*) distinguished by a single-peak profile, and an unstable branch (corresponding to larger ϕ^*) that has a more pronounced oscillation as χN increases. The latter branch ultimately connects to the small-amplitude solutions described in the previous subsection.

Solutions near the bifurcation point were computed numerically. These were obtained by dynamical steepest descents, subject to a constraint of the form (3.4), using

$$\phi_t = \left[\frac{\delta F}{\delta \phi}\right]_{xx} + \lambda(t)u_{xx}. \tag{3.32}$$

The dynamical Lagrange multiplier $\lambda(t)$ was chosen at each timestep to maintain (3.4). Note that multiplying both sides of equation (3.32) by $\phi - f$ and integrating gives an

https://doi.org/10.1017/S0956792511000398 Published online by Cambridge University Press

implicit formula for λ,

$$0 = \frac{d}{dt}\int \frac{1}{2}(\phi - f)^2 dx = \int (\phi - f)\left[\frac{\delta F}{\delta \phi}\right]_{xx} dx + \lambda(t)\int u u_{xx}\, dx. \tag{3.33}$$

Figure 3 compares the minimum value ϕ^* of the approximate solutions to the minima of numerically computed equilibria. As f decreases, the nose of the bifurcation becomes closer to the asymptotic calculation.

3.4 Intermediate region: Stable branch

When $\chi N \sim f^{-2}$ instead of f^{-1} and $\chi N \ll \chi N_s$, one may find solutions that have a 'mesa'-type profile. We construct these as in the previous subsection as an inner and outer region connected by a narrow interface. The smaller amplitude branch of the bifurcation curve also continues into this region, and ultimately connects to the small-amplitude branch. The interest here is simply showing existence of solutions by a formal construction.

The outer solution is similar to the previous case. Note that $\chi N < (\chi N)_s$ implies that $(a^1/f^2 - 2\chi N)^2/4 - \gamma < 0$, which means that if one wishes to investigate a family of solutions as $f \to 0$, we need

$$2\chi N < \frac{a_1}{f^2}. \tag{3.34}$$

With $\phi \sim f$, $x = Z f^{-1/2}$, the leading order balance is

$$f\left(Q'(\phi)\right)_{ZZ} + \gamma(f - \phi) = 0, \quad Q'(\phi) \equiv -\frac{a_1}{\phi} - 2\chi N \phi. \tag{3.35}$$

By virtue of equation (3.34), Q is convex in the relevant region $\phi \leqslant f$. Therefore, $w = Q'(\phi)$ defines a one-to-one change of variables whose inverse is given by the Legendre transform

$$\phi = P'(w), \quad P(w) = \min_{\phi}[Q(\phi) - \phi w], \tag{3.36}$$

and equation (3.35) becomes

$$w_{ZZ} + \gamma(f - P'(w)) = 0, \quad P'(w) = \frac{-w + \sqrt{w^2 - 8\chi N a_1}}{4\chi N}. \tag{3.37}$$

Integration gives

$$\frac{1}{2}w_Z^2 + \gamma(f(w - w_0) - P(w) + P(w_0)) = 0, \quad w_0 = Q'(f). \tag{3.38}$$

As before, a further integration requires the matching value $\phi^* \equiv \lim_{Z\to 0}\phi(Z)$ to provide the boundary condition $w(0) = Q'(\phi^*)$. The solution in the original variable can therefore be written as $\phi = P'(w(Z;\phi^*))$, where, in particular, ϕ is monotone increasing in Z and decreasing in the parameter ϕ^*. We will show that ϕ^* is uniquely determined and is in the relevant range $\phi < f$ for a solution of equation (3.38) to exist.

The intermediate region uses the re-scaled variable $\zeta = f^{-1}(x - z^* f^{1/2})$, where z^* is the width of the inner region to be determined, and ϕ is $\mathcal{O}(1)$. After two integrations (using

https://doi.org/10.1017/S0956792511000398 Published online by Cambridge University Press

matching conditions $\phi_\zeta = 0 = \phi_{\zeta\zeta\zeta} = 0$ as $\zeta \to \pm\infty$), the leading order equation is

$$-af^{-2}\phi_{\zeta\zeta} - \frac{a_1}{\phi} + \frac{a_1}{1-\phi} - 2\chi N\left(\phi - \frac{1}{2}\right) = 0, \tag{3.39}$$

which is subject to matching conditions $u_\zeta \to 0$ as $\zeta \to \pm\infty$. (Note that the a_1 terms are not necessarily sub-dominant if $\phi, 1-\phi = \mathcal{O}(f)$). This is the standard 'double-well' diffuse interface problem, whose solution is given by a heteroclinic orbit of this integrable system with asymptotic values corresponding to the potential minima:

$$\lim_{\zeta\to\pm\infty} \phi(\zeta) = \frac{1}{2} \mp \sqrt{\frac{1}{4} - a_1/\chi N}. \tag{3.40}$$

In particular, $\phi^* \sim a_1/\chi N$ as $f \to 0$, which provides an admissible boundary condition for the outer solution.

By virtue of matching to the intermediate layer, the inner problem necessarily has the scaling $1-\phi = \mathcal{O}(f^2)$. Together with the scaled variable $z = f^{-1/2}x$ the dominant terms are

$$\left(\frac{a_1}{1-\phi} - 2\chi N\phi\right)_{zz} = 0, \quad 0 < z < z^*,$$

which means the solution is merely a constant $\phi(z) = 1 - \phi^* \sim 1 - a_1/\chi N$ as $f \to 0$. The scaled width z^* of this region is uniquely determined by the same solvability argument used before, which reads

$$f\int_0^{z^*} \phi(z)dz = \int_0^\infty \Big(f - \phi(Z)\Big)dZ. \tag{3.41}$$

3.5 Intermediate region: Unstable branch

The continuation of the smaller amplitude branch that comes out of the bifurcation described in Section 3.3 can also be constructed in an asymptotic fashion in the intermediate regime $\chi N \sim f^{-2}$. The goal as in the previous section is to simply demonstrate the construction of a unique solution.

Observe that in the bifurcation equation (3.31), it is the larger solution of ϕ^* which corresponds to the branch of interest, and as χN becomes large, $\phi^* \to f$. Expanding $\phi^* = f + \phi_1^*$, equation (3.31) implies the scaling $\phi_1^* \sim \gamma^{1/2}(\chi N)^{-3/2} \sim f^{5/2}$. This motivates the rescaling $\phi = f - f^{5/2}\phi_1(Z)$ in the outer region described by the scaled variable $x = Zf^{-1/2}$. The dominant terms are

$$(a_1/f^2 - 2\chi N)(\phi_1)_{ZZ} - f^{-1}\gamma\phi_1 = 0, \quad \lim_{Z\to\infty} \phi_1(Z) = 0, \tag{3.42}$$

which gives the immediate solution

$$\phi_1(Z) = \phi_1^* \exp\left(-Z\sqrt{\frac{f\gamma}{a_1 - 2f^2\chi N}}\right), \tag{3.43}$$

where ϕ_1^* is yet undetermined.

https://doi.org/10.1017/S0956792511000398 Published online by Cambridge University Press

There is just one inner region, employing the scaled variable $\zeta = x/f$ and with $\phi = \mathcal{O}(f)$. To leading order one has

$$-af^{-2}\phi_{\zeta\zeta\zeta\zeta} + \left(-\frac{a_1}{\phi} - 2\chi N\phi\right)_{\zeta\zeta} = 0, \tag{3.44}$$

which is solved with the boundary conditions

$$\lim_{\zeta\to\infty}\phi(\zeta) = f, \quad \lim_{\zeta\to\infty}\phi_\zeta(\zeta) = 0 = \phi_\zeta(0) = \phi_{\zeta\zeta\zeta}(0). \tag{3.45}$$

This can be immediately integrated twice, and once more since it is Hamiltonian. Applying the far-field condition, one finds

$$\frac{a}{2f^2}\phi_\zeta^2 + \ln(\phi/f) - \frac{\phi - f}{f} + \chi N(\phi - f)^2 = 0. \tag{3.46}$$

This implicitly defines a unique homoclinic solution with even symmetry and $\phi(\zeta) > f$. The selection of ϕ_1^* proceeds as in previous cases, arising from the solvability condition demanded by volume balance:

$$\int_0^\infty (\phi(\zeta) - f)d\zeta = f\int_0^\infty \phi_1 dZ = \phi_1^*\sqrt{\frac{a_1 - 2\chi N f^2}{f\gamma}}. \tag{3.47}$$

3.6 The upper bifurcation point

When $\chi N \approx \chi N_s$, the solution for large x is not monotone as described by the outer expansion (3.35). To capture the oscillation, set $u \equiv \phi - f$, so that for small u

$$-au_{xxxx} + \beta u_{xx} - \gamma u = 0, \quad \beta \equiv a_1/f^2 - 2\chi N. \tag{3.48}$$

If all three terms are to be retained in the dominant balance for small f, then lengths must be scaled as $z = x/f^{1/4}$ and $\beta = \mathcal{O}(f^{-1/2})$.

To match the linear oscillatory region to the outer solution defined by equation (3.35), one needs $u = \mathcal{O}(f^{5/2})$, and the leading order equation is (in unscaled variables)

$$-au_{xxxx} - 2\frac{a_1}{f^3}(u^2)_{xx} + \beta u_{xx} - \gamma u = 0. \tag{3.49}$$

Non-dimensionalising by

$$z = (\gamma/a)^{1/4}x, \quad U = \frac{2a_1}{f^3(a\gamma)^{1/2}}u, \quad \Gamma = -\frac{\beta}{(a\gamma)^{1/2}}, \tag{3.50}$$

equation (3.49) becomes

$$U_{zzzz} + \Gamma U_{zz} + U + (U^2)_{zz} = 0. \tag{3.51}$$

The solution must decay as $z \to \infty$, and must become unbounded as $z \to -\infty$ in order

https://doi.org/10.1017/S0956792511000398 Published online by Cambridge University Press

to match the outer solution. Note that when the non-dimensional quantity $\Gamma \to 2$, $\chi N \to (\chi N)_s$.

The oscillatory solutions must match to a region of no oscillation, where u has size $\mathcal{O}(f^\alpha)$ with $1 < \alpha < 5/2$. Using a similar non-dimensionalisation as above,

$$Z = f^{5/4-\alpha/2}(\gamma/a)^{1/4}x, \quad w = \frac{2a_1}{f^{\alpha+1/2}(a\gamma)^{1/2}}u, \tag{3.52}$$

and it is found to leading order that

$$(w^2)_{ZZ} + w = 0. \tag{3.53}$$

It is straightforward to match the w and U approximations, which leads to the conditions

$$w(Z^*) = 0 = w_Z(Z^*), \quad U(z) \sim \frac{1}{2}w_{ZZ}(Z^*)z^2, \quad z \to -\infty, \tag{3.54}$$

where Z^* is the point of crossover to the oscillatory region. The first two conditions can be used with equation (3.53) to give the exact solution $w = -(Z - Z^*)^2/12$, which implies that

$$U(z) \sim -\frac{1}{12}z^2, \quad z \to \infty. \tag{3.55}$$

The problem for U can be studied by a shooting method. There are two modes for the linearisation of equation (3.51) which decay as $z \to \infty$. Writing $\eta = (U, U_z, U_{zz}, U_{zzz})$, let η_1, η_2 span the linear stable manifold of $\eta = 0$. The idea is to find a trajectory on the (nonlinear) stable manifold which has the correct asymptotic behaviour (3.55).

A numerical implementation is as follows. A small initial condition $\eta(0) = \epsilon[\cos(\theta)\eta_1 + \sin(\theta)\eta_2]$ near the stable manifold is chosen, and the integration proceeds backwards in z until $|U|$ is larger than some tolerance $U_{max} \gg 1$ (it was found that $\epsilon = 0.05$ and $U_{max} = 4$ gave satisfactory results). The condition (3.55) can be encoded as $U_{zzz} = 0$ as $z \to -\infty$. The problem therefore becomes one of finding θ so that $U_{zzz} = 0$ when $|U| = U_{max}$, which was solved by a combination of a line search and bisection.

Figure 4 shows the results for $\Gamma = 1.7$ and $\Gamma = 1.87$. There are two distinct solutions for U in the former case. As Γ is increased, the θ values of these solutions become closer, until $\Gamma_b \approx 1.87$, where the two solutions are nearly indistinguishable (Figure 4). This suggests a saddle-node bifurcation is imminent near this parameter value.

In terms of the original variables, this predicts the upper bifurcation point is related to the point of spinodal instability by

$$(\chi N)_s - (\chi N)_{SR} = \frac{1}{2}(2 - \Gamma_b)\sqrt{a\gamma}. \tag{3.56}$$

For $f = 0.1, \gamma = 72, a = 2.34$, we find that the exact values are $(\chi N)_s = 72.37$ and $(\chi N)_{SR} = 71.36$ whereas formula (3.56) yields $(\chi N)_s - (\chi N)_{SR} = 0.9$.

3.7 Multi-peaked solutions

More complex equilibria can be built from the stable and unstable structures previously described. This viewpoint has been used in a dynamical setting [14, 17, 45] using

https://doi.org/10.1017/S0956792511000398 Published online by Cambridge University Press

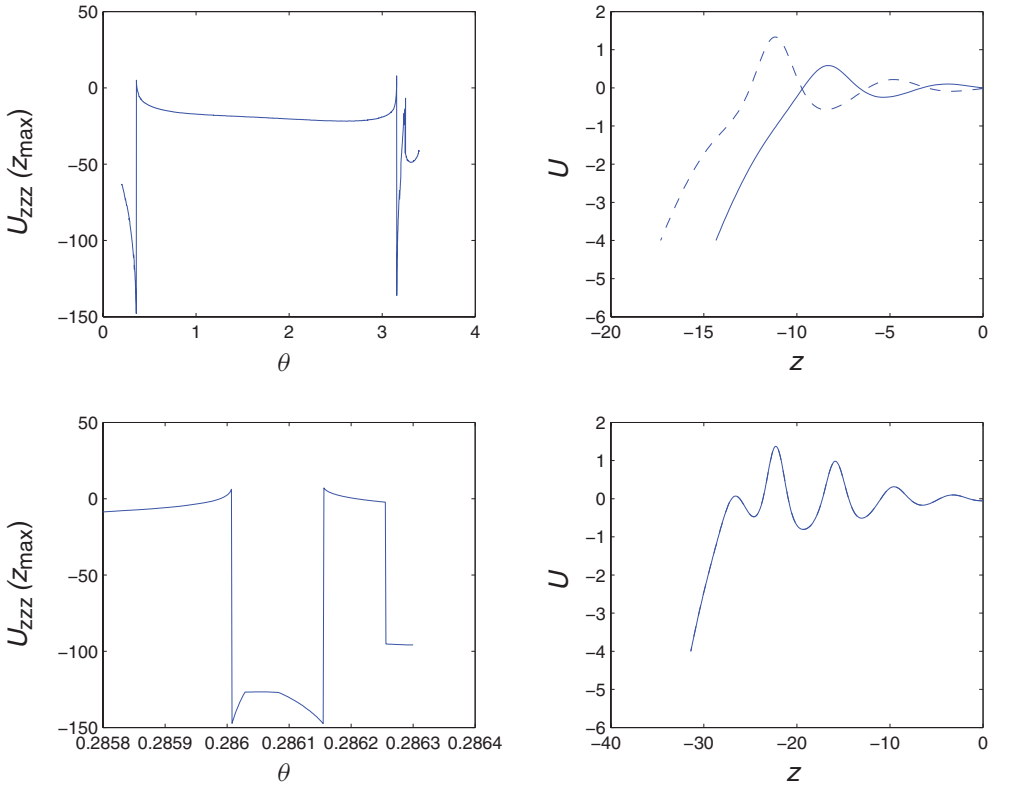

FIGURE 4. (Colour online) Results of the shooting method applied to equation (3.51). The top figure is for $\Gamma = 1.7$, showing the shooting function U_{zzz} at the exit point $U = U_{max}$ as a function of θ. Two distinct values $\theta \approx 0.3650565, 3.1545$ yield the solutions (solid, dashed respectively) shown on the right. The lower figures are for $\Gamma = 1.87$. In this case, the values $\theta \approx 0.286207, 0.285988$ give nearly indistinguishable solutions (right), suggesting an imminent bifurcation.

perturbation methods. The basic idea is an ansatz

$$\phi(x,\tau) = f + \sum_{i=1}^{n} (\phi_0(x - x_i(\tau)) - f) + \epsilon\psi(x,\tau), \quad \tau = \epsilon t, \tag{3.57}$$

where ψ is a correction term and ϕ_0 is a single-peak equilibrium solution with its maximum at $x = 0$. As long as the locations x_i are sufficiently separated, the correction term has size $\epsilon \sim \exp(-L)$, where L is the characteristic separation distance. This analysis produces a system for dx_i/dt with nearest neighbour interaction. In the case where the far-field behaviour of solutions is oscillatory, this takes the form [17] (assuming the positions are ordered $x_1 < x_2 < x_3 < \ldots$)

$$\frac{dx_i}{d\tau} = F(x_{i+1} - x_i) - F(x_i - x_{i-1}), \quad F(x) = I \exp(-[Re\lambda]x) \sin([Im\lambda]x - \alpha). \tag{3.58}$$

Here, I is a positive integral that depends on ϕ_0, and α is a phase shift that can be ascertained from the structure of ϕ_0 (if there is no left or right neighbour, the

https://doi.org/10.1017/S0956792511000398 Published online by Cambridge University Press

corresponding term is ignored). As $\tau \to \infty$, steady states may be reached which exhibit 'mode lock'. This is characterised by peak separation distances that are multiples of the oscillation wavelength $2\pi/Im\lambda$, up to some phase shift.

If, instead, the far-field behaviour is characterised by exponential decay, peak locations still obey a nearest neighbour interaction of the form (3.58a), except $F(d) < 0$ if $d > 0$ and the interaction is strictly repulsive. This means multi-peak equilibria that exist for $\chi N > (\chi N)_{osc}$ would break up as χN is decreased past $(\chi N)_{osc}$. This is somewhat of an artefact of using an infinite domain; in a sense, the bifurcation curves "go to infinity" at $\chi N = (\chi N)_{osc}$. Thus, true multi-peaked equilibria don't exist for $\chi N > (\chi N)_{osc}$. One could, in principle, obtain a continuous bifurcation picture by working on a finite domain instead, although this is not pursued here.

One would expect equation (3.57) to make sense as a large time approximation only if ϕ_0 were stable. Steady solutions, however, can be built by "gluing" together stable ϕ^S and unstable ϕ^U single peaks (assuming χN is in the range where they both exist):

$$\phi(x) = f + \sum_{i=1}^{n} \left(\phi_0^{\mathscr{S}_i}(x - x_i) - f\right) + \mathcal{O}(\epsilon), \qquad \mathscr{S}_i \in \{S, U\}. \tag{3.59}$$

The calculation of peak locations x^i proceeds exactly as in [17]; the details are recounted in the Appendix. The conclusion is a set of equations with nearest neighbour coupling

$$0 = F(x_{i+1} - x_i; \mathscr{S}_i, \mathscr{S}_{i+1}) - F(x_i - x_{i-1}; \mathscr{S}_i, \mathscr{S}_{i-1}), \tag{3.60}$$

where a term with index i is suppressed if $i \neq 1, 2, \ldots, n$. The $\mathscr{S}$ dependency in the interaction functions F accounts for whether neighbouring peaks are stable or unstable. As with the dynamical interaction, F oscillates if and only if $\chi N > (\chi N)_{osc}$.

From here onward, we will focus on the case of even solutions on the half line $[0, \infty)$ with the first peak fixed at $x = 0$. The following notation will be adopted: S will denote a stable peak, U an unstable one, and even multi-peaked states are described by a string $\mathscr{S}_1\mathscr{S}_2\mathscr{S}_3 \ldots \mathscr{S}_n$, where $\mathscr{S}_1$ is the stability of the peak located at $x = 0$. (This could be equivalently regarded as a state $\mathscr{S}_n \ldots \mathscr{S}_3\mathscr{S}_2, \mathscr{S}_1\mathscr{S}_2\mathscr{S}_3 \ldots \mathscr{S}_n$ on the whole real line.)

For the case where F oscillates, one can construct any combination $\mathscr{S}_1\mathscr{S}_2 \ldots \mathscr{S}_n$. This is done by first determining the spacing of the right-most peak

$$F(x_n - x_{n-1}; \mathscr{S}_{n-1}, \mathscr{S}_n) = 0, \tag{3.61}$$

and then proceeding inductively to find the remaining spacings

$$F(x_{i-1} - x_{i-2}; \mathscr{S}_{i-2}, \mathscr{S}_{i-1}) = F(x_i - x_{i-1}; \mathscr{S}_i, \mathscr{S}_{i-1}) = 0, \quad i = n-1, n-2, n-3, \ldots \tag{3.62}$$

For each i, there are many solutions; in what follows, we consider only those for which the spacing $x_i - x_{i-1}$ is as small as possible so that the dynamical interaction (3.58) is stable

For finite domains, the argument is somewhat more subtle. If the domain is large compared to the number of peaks, the exponentially decaying interaction of the right-most peak and right boundary can be ignored, and the previous construction is asymptotically

https://doi.org/10.1017/S0956792511000398 Published online by Cambridge University Press

correct. As χN is taken down towards $(\chi N)_{osc}$, the preferred spacing of peaks becomes large (since the imaginary part of the eigenvalue corresponding to spatial decay goes to zero), and the interaction with the right boundary becomes important. Nevertheless, the solution branch $\mathscr{S}_1\mathscr{S}_2\ldots\mathscr{S}_n$ can be continued until a bifurcation point, which is discussed in the next section.

Stability of the various solution branches can be studied by the linearisation of equation (2.4) about a steady solution ϕ, or equivalently by looking at the second variation of the energy. The latter involves the linear operator

$$\mathscr{L}_\phi = -\frac{d}{dx^2} - 2\chi N - G * + h''(\phi) \equiv \mathscr{L}_0 + h''(\phi). \tag{3.63}$$

For the single unstable peak $\phi = \phi^U$, it was shown (Section 3.1) that there is a single unstable eigenfunction η^U. By virtue of linearisation at infinity, it can be seen that η^U has the same exponential decay rate as ϕ_0. If there is at least one unstable peak when $i = j$ in equation (3.59), then the Rayleigh integral is

$$\begin{aligned}
&\int \eta^U(x - x_j)\mathscr{L}_\phi \eta^U(x - x_j)dx \\
&= \int \eta^U(x - x_j)\mathscr{L}_0 \eta^U(x - x_j)dx \\
&\quad + \int \eta^U(x - x_j)h''\left(\sum_{i=1}^{n}\left(\phi_0^{\mathscr{S}_i}(x - x_i) - f\right)\right)\eta^U(x - x_j)dx \\
&= \int \eta^U(x - x_j)\mathscr{L}_0 \eta^U(x - x_j)dx \\
&\quad + \int \eta^U(x - x_j)h''(\phi^U(x - x_j))\eta^U(x - x_j)dx + \mathscr{O}(\epsilon) \\
&= \int \eta^U \mathscr{L}_{\phi^U}\eta^U\, dx + \mathscr{O}(\epsilon).
\end{aligned} \tag{3.64}$$

Thus, the approximate superposition (3.59) is also unstable as long as the negative eigenvalue of $\mathscr{L}_{\phi^U}$ is not exponentially small.

If equation (3.59) is composed of only stable peaks, then one must consider the role of interaction (2.4). The eigenvalues more or less divide into two categories [46]: order 1 eigenvalues associated with the stability of a single peak, and exponentially small eigenvalues which can be ascertained perturbatively from linearisation of the reduced dynamics (2.4). We will suppose that the $SSS\ldots$ branches under consideration are strictly those formed by stable interactions. Existence of these types of solutions were explored previously [17].

4 Self-replication

4.1 The global bifurcation diagram

The previous section derived local solution branches that form the connected fundamental branch. The small-amplitude solutions grow as χN is reduced, pass through the intermediate region and bifurcate at the fold point $(\chi N)_{MD}$. As χN then increases along the stable

https://doi.org/10.1017/S0956792511000398 Published online by Cambridge University Press

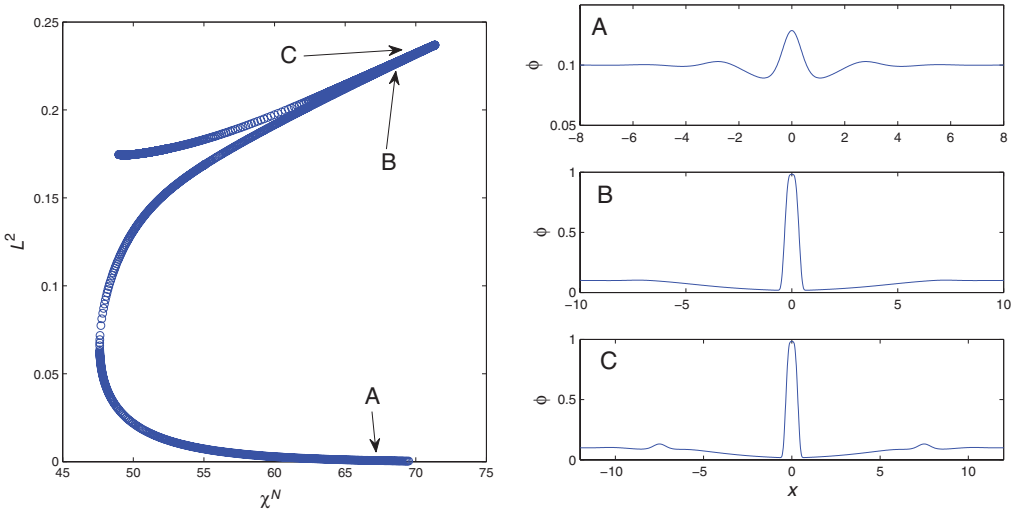

FIGURE 5. (Colour online) Numerical continuation of the primary (one peak) branch of steady states. The vertical axis represents the L^2 norm of $\phi - f$. Small-amplitude solutions (A) grow and bifurcate to create the stable branch (B). This branch then bifurcates at $(\chi N)_{SR}$ and creates a solution (C) which is an approximate superposition of small-amplitude unstable peaks and a stable peak in the middle.

branch, the intermediate region is passed leading to the parameter region described by the upper bifurcation point. The continuation of this branch past the upper bifurcation point $(\chi N)_{SR}$ is less clear.

To explore this issue, we use numerical pseudo-arclength continuation [1] to compute solutions of (3.1) past the fold point. The results for even symmetry solutions are shown in Figure 5. The calculation suggests that the route the bifurcation takes is to 'glue' an unstable branch solution on each side of the stable peak. As χN is further reduced, the outlying peaks grow until the next fold point χ_{MD} is reached. At this point, all three peaks are essentially the same size, and each is at the transition from stable to unstable. This point is the intersection of two *different* branches: one describing the $SU \to US$ transition and the other describing the $UU \to SS$ transition (see Figure 6).

The same reasoning can lead to a repeated construction of different branches labelled by a string of S and U symbols. Thus, the SS branch bifurcates at $(\chi N)_{SR}$ to the SSU branch, which continues (with χN decreasing) until the merger with the UUU, UUS, USU, USS, SUU, SUS and SSS branches. Note that we could also construct other solution branches for which the spacing between peaks was not minimal (e.g. adding other multiples of the tail oscillation frequency), but we avoid that complexity here.

4.2 Dynamic pathways

Certain qualitative aspects of dynamics (equation (2.4)) can also be inferred from the global bifurcation diagram, at least in a region of parameter space near the interval $(\chi N)_{MD} \leqslant \chi N \leqslant (\chi N)_{SR}$. The reasoning relies on persistence of heteroclinic orbits (in the time-dependent PDE sense) connecting unstable and stable states. One must verify or

https://doi.org/10.1017/S0956792511000398 Published online by Cambridge University Press

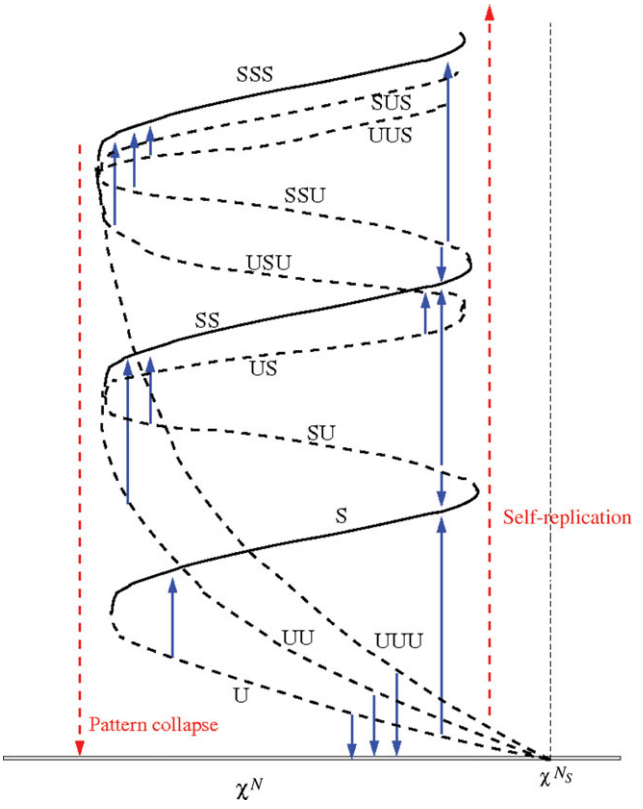

FIGURE 6. (Colour online) Sketch of the global bifurcation diagram for even-symmetry solutions and corresponding dynamic pathways. The fundamental stable and unstable branches near the bottom are labelled U and S. The other branches are predicted by the singular perturbation calculation derived from the approximate superposition of single-peak solutions. By virtue of the stability of various branches, heteroclinic pathways leading from unstable to stable branches can be inferred (represented schematically by solid arrows). Past the lower $(\chi N)_{MD}$ or upper $(\chi N)_{SR}$ bifurcation points, one expects the dynamical pathways to persist, leading to pattern collapse or self-replication (the vertical axis is an arbitrary coordinate).

otherwise accept that as the bifurcation parameter χN changes, these orbits continuously deform and remain qualitatively intact.

Heteroclinic pathways are created, in a sense, at the bifurcation points. For example, by virtue of stability of the SS state, near $(\chi N)_{MD}$ there are trajectories leading from the SU, US and UU branches (in Figure 6, these are the solid arrows). If these pathways persist as χN increases, this implies a connection between the SU and SS branches near the upper bifurcation point $(\chi N)_{SR}$. There is also a complementary heteroclinic connection between the SU and S branches near $(\chi N)_{SR}$, so there is consequently a pathway connecting them even near $(\chi N)_{MD}$. The conclusion is that a perturbation of the (unstable) SU state would likely do one of two things: either proceed towards the stable peak S by shedding outlying peaks, or move towards SS by growth of the outlying peaks.

https://doi.org/10.1017/S0956792511000398 Published online by Cambridge University Press

4.3 Self-replication and pattern collapse

Just beyond the bifurcation points, localised states give way to dynamical phenomena. It was shown in [17] that the free energy of a single peak becomes negative (relative to the flat state) as χN is increased. Adiabatically increasing χN past $(\chi N)_{SR}$ must therefore lead to pattern propagation, rather than collapse towards the homogeneous state $\phi = f$. This propagation takes the form of *self-replication* of individual peaks outward in space. This phenomenon has been commonly observed and studied in a variety of models [12, 23, 30, 35, 37].

There are two commonly observed scenarios for self-replication. One is where peaks appear to split apart, sometimes termed 'pulse splitting' [23]. In contrast, our situation is like 'edge-splitting' [22] or 'peak insertion' [33], where peaks nucleate from the homogeneous state rather instead. It should be emphasised that this phenomenon is distinct from propagation into an unstable homogeneous state since χN may be below the spinodal instability threshold.

A basic explanation for self-replication in pattern-forming systems was put forward by Nishiura and Ueyama (NE) [30]. Their idea is that self-replication dynamics are an 'aftereffect' of simultaneous (or nearly simultaneous) saddle-node bifurcations. When the fixed points disappear, there are still attractive orbits passing close to the saddle-node bifurcations. Provided these orbits lead approximately from one bifurcation point to another, one expects dynamics which appear to create new near-equilibrium structures.

In our problem, the upper bifurcation points of all multi-peak states are approximately $(\chi N)_{SR}$, simply as a result of the cut-and-paste construction which utilises the single-peak solution. This, of course, does not preclude the possibility that the multi-peak solutions might persist just above $(\chi N)_{SR}$, but these states would have to be outside of the range of validity of the perturbation expansion. The upper bounds for existence (in χN) for the S, SS and SSS stable solutions were checked numerically and found to be almost exactly the same. This seems to be a special feature of our problem. Indeed, it has been observed elsewhere (e.g. [30]) that the fold points are often not perfectly aligned, but form a sort of cascade structure where the domain of existence expands as the bifurcation diagram is traversed upwards.

The other ingredient in self-replication is the requirement that a dynamically relevant trajectory (that is, one which attracts a large set) leads from one state to another. In other words, one must have a pathway that closely proceeds as $S \to SS \to SSS \to \ldots$. The justification for this comes from extending the heteroclinic orbits from the unstable branches to the stable ones (the solid arrows in Figure 6), just past the bifurcation point. Starting from an initial condition near the single peak S, the dynamics would seem to jump on the heteroclinic branch connecting SU to SS, which is described by the growth of a peak to the right of the first large one. This is precisely what is seen in numerical experiments (Figure 7).

It is also interesting to ask what happens in the reverse case, when χN is decreased below $(\chi N)_{MD}$. There are heteroclinic orbits which connect the multi-peaked unstable branches U, UU, UUU etc., to the homogeneous state $\phi = f$. The continuation of these orbits past the bifurcation point does not lead to a single pathway of the form $UUU \to UU \to U$ but rather many *distinct* paths, all of which lead directly from an

https://doi.org/10.1017/S0956792511000398 Published online by Cambridge University Press

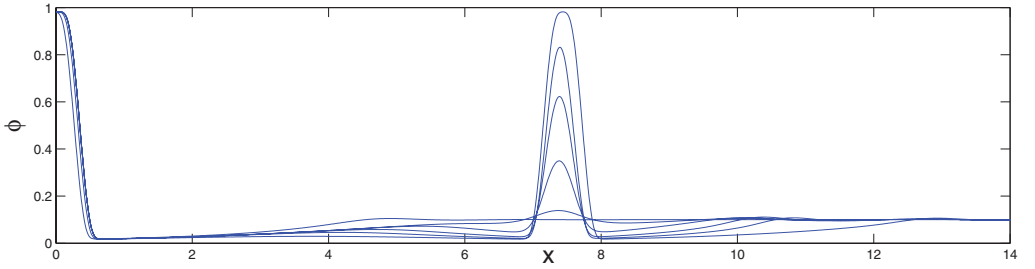

FIGURE 7. (Colour online) Numerical evolution of self-replication ($\chi N = 71.5$, $f = 0.1$, $\gamma = 72$). The initial condition was found by setting $\chi N = 70 < (\chi N)_{SR} \approx 71.4$ and relaxing to a single-peaked equilibrium. The dynamics lead to the creation of a rapidly growing outlying peak at about $x = 7.5$.

N-peak state to the flat state. Therefore, one expects collapse of the pattern, rather than self-replication in reverse. This is corroborated by numerical experiments.

4.4 Scaling of self-replication velocity

We conclude the discussion of self-replication by a numerical study of the velocity of pattern propagation as a function of the parameter χN. Near the onset of self-replication, the dynamics are multi-scale: they are slow between self-replicating events, where small outlying peaks take a long time to nucleate, and fast during the growth process. The passage of an orbit near a saddle-node bifurcation point is necessarily slow; in particular, the time of passage should scale as $(\chi N - (\chi N)_{SR})^{-1/2}$.

As further evidence of the NE self-replication scenario, numerical experiments were conducted to examine the rate of pattern growth from a single peak. The domain was chosen to be large enough to accommodate at least 20 peaks. Times and locations were recorded for the 'birth' of each subsequent peak, and linear regression was used to compute an average velocity. The results of this experiment are shown in Figure 8. The fit of the scaling exponent was very close to the predicted value of $1/2$.

Note that two data points in Figure 8 are for $\chi N > (\chi N)_s$. In this case, the pattern is propagating into an unstable flat state instead. This appears to be different than propagation into an unstable state predicted by linear mechanisms (e.g. [11, 42]). In particular, the propagation speed is non-zero as the point of instability is crossed.

5 Conclusion

Localised states in models of block co-polymers have a complex, inter-connected bifurcation diagram. One can infer dynamics from the global picture, and draw conclusions about the mechanisms that lead from a disordered arrangement of localised structures to a patterned state. This lends some clarity to the theoretical description of heterogeneous structures that appear independently of spinodal decomposition.

Physically, the one-dimensional equilibria studied correspond to three-dimensional bilayers of infinite extent. This case was the main focus of this paper, since many of the calculations can be made explicitly. One finds a similar description for 2-D axisymmetric and 3-D spherical localised states [17], corresponding to cylindrical and spherical

https://doi.org/10.1017/S0956792511000398 Published online by Cambridge University Press

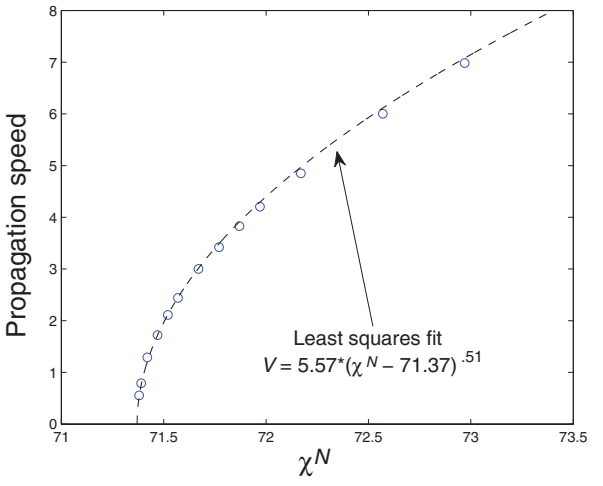

FIGURE 8. (Colour online) Speed of self-replication, obtained by linear regression of peak growth events. Also shown is a power law fit giving scaling exponent ≈ 0.51. ($f = 0.1$, $\gamma = 72$).

micelles respectively. The higher dimensional analogue of multi-peak solutions are micelle clusters, which can be predicted by the exponentially small interaction of individual micelles. Self-replication can also be seen in higher dimensions, but it is complicated by other instabilities in micellar structures themselves [17].

There has been an ongoing discussion in the literature about the nature of the order–disorder transition for block co-polymers [13,34,43]. Central to this issue is the appearance of states with no long-range order (i.e. disordered micelles). An outstanding question is how to characterise the multiplicity of metastable states in this regime. One approach is that of Zhang and Wang [47], who compute the configurational entropy [28] in a density functional model. Their conclusions indicate that for highly asymmetric volume fractions, there can be a glass transition which occurs at temperatures above the spinodal. This is consistent with our picture of a multiplicity of metastable equilibria, at least up to the point of self-replication. This phenomenon suggests a transition to equilibria which are space-filling patterns with some degree of ordering, instead of being trapped in a single metastable glass-like state, however.

One physically important phenomenon which is lacking in the present description are fluctuations which describe deviations from the mean-field approximation. There are systematic ways of including these into equilibrium descriptions of block co-polymers [16], but less has been done incorporating them into a dynamical theory. One might consider an ad-hoc approach, allowing for stochastic motion and nucleation of individual structures within a reduced dynamical description. This would allow for aggregation and/or self-organisation of micelle clusters by virtue of interaction dynamics. Additionally, nucleation of new structures would be expected near the self-replication threshold, since the free energy barriers between multi-peak states become small. In this sense, self-replication might be preempted by fluctuation-driven nucleation.

The ingredients we identify that culminate in self-replication dynamics are not particular to block co-polymers. The central features which generate this phenomenon are (1) a

https://doi.org/10.1017/S0956792511000398 Published online by Cambridge University Press

sub-critical bifurcation of a single elementary localised state giving rise to an unstable and stable branch, (2) the ability to glue together stable and unstable localised states, (3) the simultaneous loss of all localised states at some upper bifurcation point. These phenomena are very common throughout the literature on pattern-forming systems [9].

A complete description of the order–disorder transition in three dimensions is much more complicated by virtue of other instabilities that arise. In two dimensions, these take the form of micelles which deform as growing filaments, which themselves may become unstable [17]. A more detailed examination of these dynamical modes may lead to a better understanding of the morphology that is observed in the ordered regime as well.

Appendix

Details leading to equation (3.60) are now given. The calculation proceeds as in [14, 17]. Starting from equation (3.59), the correction term solves the linear equation

$$\mathscr{L}\psi = -\epsilon^{-1}R_{xx}, \quad R \equiv N\left(f + \sum_{i=1}^{n}(\phi_i^{\mathscr{S}_i} - f)\right) - \sum_{i=1}^{n} N(\phi_i - f), \tag{A1}$$

where $\phi_i = \phi_0(x - x_i)$ has been used and N_{xx} is the non-linear part of the equation for ϕ^S or ϕ^U:

$$\begin{aligned} -a\phi_{xxxx} + [g''(f)(\phi - f) + N(\phi)]_{xx} + \gamma(f - \phi) &\equiv \mathscr{L}\phi + N(\phi), \\ N(\phi) &\equiv g'(\phi) - g''(f)(\phi - f) - g'(f). \end{aligned} \tag{A2}$$

Note the R term is actually $\mathscr{O}(\epsilon)$.

One obtains a solvability condition for equation (A1) using the approximate eigenfunctions $\eta^{\mathscr{S}}, \mathscr{S} = S, U$ satisfying

$$-a(\eta^{\mathscr{S}})_{xxxx} + g''(\phi_0^{\mathscr{S}})\eta_{xx}^{\mathscr{S}} - \gamma\eta^{\mathscr{S}} = 0, \tag{A3}$$

together with an appropriate decay condition for $|x| \to \infty$. In one dimension, these are explicitly

$$\eta^{\mathscr{S}}(x) = \int_{-\infty}^{x} \phi_0^{\mathscr{S}}(x')\,dx'. \tag{A4}$$

Note that η has the same decay rate in the far field as ϕ_0.

Multiplying equation (A1) by $\eta^{\mathscr{S}_l}(x - x_l)$, $l = 1, 2, \ldots, n$, and integrating over the real line, at leading order one gets

$$0 = \sum_{i \neq l} \frac{\int N'(\phi_l^{\mathscr{S}_l})(\phi_i^{S_i} - f)(\phi_l^{\mathscr{S}_l})_x\,dx}{\int (\phi_l^{\mathscr{S}_l})_x \eta^{\mathscr{S}_l}(x - x_l)dx}. \tag{A5}$$

The far-field behaviour of equilibria (3.1) can be written as

$$\phi_0^{\mathscr{S}} - f \sim Re\left[A^{\mathscr{S}} \exp(-Q^{\mathscr{S}}x)\right], \quad x \to \infty,$$

https://doi.org/10.1017/S0956792511000398 Published online by Cambridge University Press

where A may be complex. Since the numerator of (A5) has an order 1 factor and a factor which can be approximated by the exponentially small tail of ϕ_0, for $x_l > x_j$ this integral approximates to

$$Re\left[\int A^{\mathscr{S}} \exp(-Q^{\mathscr{S}}(x-x_j))N'(\phi_l^{\mathscr{S}_l})(\phi_l^{\mathscr{S}_l})_x dx\right] = Re\left[A^{\mathscr{S}} I^{\mathscr{S}} \exp(Q^{\mathscr{S}}(x_j - x_l))\right],$$
$$I^{\mathscr{S}} \equiv \int \exp(-Q^{\mathscr{S}} x)N'(\phi_0^{\mathscr{S}})(\phi_0^{\mathscr{S}})_x\, dx. \tag{A6}$$

Since all these integrals are $\mathscr{O}(\epsilon^2)$ except for those involving the nearest neighbours, equation (A5) reduces to equation (3.60) with

$$F(x; \mathscr{S}_i, \mathscr{S}_{i+1}) = Re\left[J \exp(-Q^{\mathscr{S}_i} x)\right], \quad J \equiv \frac{A^{\mathscr{S}_{i+1}} I^{\mathscr{S}_{i+1}}}{\int (\phi_0)_x \eta^{\mathscr{S}_{i+1}}\, dx}. \tag{A7}$$

Acknowledgements

The author has benefitted from conversations with Zhen-Gang Wang and Steven Rosenthal. This work was supported under NSF award DMS-0405596.

References

[1] Allgower, E. L. & Georg, K. (2003) *Introduction to Numerical Continuation Methods*, SIAM Classics in Applied Mathematics, Society for Industrial and Applied Mathematics, Philadelphia.

[2] Bates, F. S., Rosedale, J. H. & Fredrickson, G. H. (May 1990) Fluctuation effects in a symmetric diblock copolymer near the order–disorder transition. *J. Chem. Phys.* **92**, 6255–6270.

[3] Bates, F. S. & Fredrickson, G. H. (1999) Block copolymers – designer soft materials. *Phys. Today* **52**, 32–38.

[4] Beck, M., Knobloch, J., Lloyd, D. J. B., Sandstede, B. & Wagenknecht, T. (2009) Snakes, ladders, and isolas of localized patterns. *SIAM J. Math. Anal.* **41**(3), 936–972.

[5] Bohbot-Raviv, Y. & Wang, Z.-G. (October 2000) Discovering new ordered phases of block copolymers. *Phys. Rev. Lett.* **85**(16), 3428–3431.

[6] Budd, C. J., Hunt, G. W. & Kuske, R. (December 2001) Asymptotics of cellular buckling close to the Maxwell load. *R. Soc. Lond. Proc. Seri. A* **457**, 2935–2964.

[7] Chapman, S. J. & Kozyreff, G. (February 2009) Exponential asymptotics of localised patterns and snaking bifurcation diagrams. *Phys. D Nonlinear Phenom.* **238**, 319–354.

[8] Choksi, R. & Ren, X. (2003) On the derivation of a density functional theory for microphase separation of diblock copolymers. *J. Statist. Phys.* **113**(1–2), 151–176.

[9] Cross, M. C. & Hohenberg, P. C. (July 1993) Pattern formation outside of equilibrium. *Rev. Mod. Phys.* **65**(3), 851.

[10] Dawes, J. H. P. (July 2010) The emergence of a coherent structure for coherent structures: Localized states in nonlinear systems. *R. Soc. Lond. Phil. Trans. Seri. A* 368, 3519–3534.

[11] Dee, G. & Langer, J. S. (1983) Propagating pattern selection. *Phys. Rev. Lett.* **50**, 383–386.

[12] Doelman, A., Kaper, T. J., & Eckhaus, W. (2000) Slowly modulated two-pulse solutions in the Gray–Scott model i: Asymptotic construction and stability. *SIAM J. Appl. Math.* **61**(3), 1080–1102.

[13] Dormidontova, E. E. & Lodge, T. P. (2001) The order–disorder transition and the disordered micelle regime in sphere-forming block copolymer melts. *Macromolecules* **34**(26), 9143–9155.
[14] Elphick, C., Meron, E. & Spiegel, E. A. (1990) Patterns of propagating pulses. *SIAM J. Appl. Math.* **50**(2), 490–503.
[15] Evans, L. C. (1998) *Partial Differential Equations*, American Mathematical Society, Providence, RI.
[16] Fredrickson, G. H. (2006) *The Equilibrium Theory of Inhomogeneous Polymers*, Oxford Science Publications, Clarendon Press, Oxford.
[17] Glasner, K. B. (2010) Spatially localized structures in diblock copolymer mixtures. *SIAM J. Appl. Math.* **70**(6), 2045–2074.
[18] Hamley, I. W. (1998) *The Physics of Block Copolymers*, Oxford Science Publications, Clarendon Press, Oxford.
[19] Hashimoto, T., Sakamoto, N. & Koga, T. (1996) Nucleation and growth of anisotropic grain in block copolymers near order–disorder transition. *Phys. Rev. E* **54**(5), 5832–5835.
[20] Helfand, E. (1975) Theory of inhomogeneous polymers: Fundamentals of the Gaussian random-walk model. *J. Chem. Phys.* **62**(3), 999–1005.
[21] Hong, K. M. & Noolandi, J. (1981) Theory of inhomogeneous multicomponent polymer systems. *Macromolecules* **14**, 727–736.
[22] Ichiro E. S., Nishiura, Y. & Ueda, K. I. (2001) 2^n-splitting or edge-splitting? A manner of splitting in dissipative systems. *Japan J. Ind. Appl. Math.* **18**, 181–205. 10.1007/BF03168570.
[23] Kolokolnikov, T., Ward, M. J. & Wei, J. (2007) Self-replication of mesa patterns in reaction–diffusion systems. *Phys. D: Nonlinear Phenom.* **236**(2), 104–122.
[24] Leibler, L. (1980) Theory of microphase separation in block copolymers. *Macromolecules* **13**, 1602–1617.
[25] Maddocks, J. H. (December 1987) Stability and folds. *Arch. Ration. Mech. Anal.* **99**, 301–328.
[26] Matsen, M. W. & Bates, F. S. (1996) Unifying weak- and strong-segregation block copolymer theories. *Macromolecules* 29, 1091–1098.
[27] Matsen, M. W. & Schick, M. (April 1994) Stable and unstable phases of a diblock copolymer melt. *Phys. Rev. Lett.* **72**(16), 2660–2663.
[28] Monasson, R. (October 1995) Structural glass transition and the entropy of the metastable states. *Phys. Rev. Lett.* **75**, 2847–2850.
[29] Nishiura, Y. & Ohnishi, I. (1995) Some mathematical aspects of the micro-phase separation of diblock copolymers. *Phys. D* **84**, 31–39.
[30] Nishiura, Y. & Ueyama, D. (June 1999) A skeleton structure of self-replicating dynamics. *Phys. D: Nonlinear Phenom.* **130**, 73–104.
[31] Ohta, T. & Kawasaki, K. (1986) Equilibrium morphology of block coploymer melts. *Macromolecules* **19**, 2621–2632.
[32] Ohta, T. & Kawasaki, K. (1990) Comment on the free energy functional of block copolymer melts in the strong segregation limit. *Macromolecules* **23**, 2413–2414.
[33] Painter, K. J., Maini, P. K. & Othmer, H. G. (May 1999) Stripe formation in juvenile Pomacanthus explained by a generalized Turing mechanism with chemotaxis. *Proc. Natl. Acad. Sci.* **96**, 5549–5554.
[34] Park, M. J., Char, K., Lodge, T. P.& Kim, J. K. (2006) Transient solidlike behavior near the cylinder/disorder transition in block copolymer solutions. *J. Chem Phys.* **110**, 15295–15301.
[35] Pearson, J. E. (July 1993) Complex patterns in a simple system. *Science* **261**, 189–192.
[36] Pomeau, Y. (December 1986) Front motion, metastability and subcritical bifurcations in hydrodynamics. *Phys. D: Nonlinear Phenom.* **23**, 3–11.
[37] Reynolds, W. N., Pearson, J. E. & Ponce-Dawson, S. (April 1994) Dynamics of self-replicating patterns in reaction diffusion systems. *Phys. Rev. Lett.* **72**, 2797–2800.
[38] Sakamoto, N., Hashimoto, T., Han, C. D., Kim, D. & Vaidya, N. Y. (1997) Order–order and order–disorder transitions in a polystyrene–block–polyisoprene–block–polystyrene copolymer. *Macromolecules* **30**(6), 1621–1632.

[39] Schwab, M. & Stühn, B. (February 1996) Thermotropic transition from a state of liquid order to a macrolattice in asymmetric diblock copolymers. *Phys. Rev. Lett.* **76**, 924–927.
[40] Semenov, A. N. (1989) Microphase separation in diblock copolymer melts: Ordering of micelles. *Macromolecules* **22**, 2849–2851.
[41] Uneyama, T. & Doi, M. (2005) Calculation of the micellar structure of polymer surfactant on the basis of the density functional theory. *Macromolecules* **38**(13), 5817–5825.
[42] Van Saarloos, W. (1988) Front propagation into unstable states: Marginal stability as a dynamical mechanism for velocity selection. *Phys. Rev. A* **37**, 211–229.
[43] Wang, J., Wang, Z.-G. & Yang, Y. (2005) Nature of disordered micelles in sphere-forming block copolymer melts. *Macromolecules* **38**(5), 1979–1988.
[44] Wang, X., Dormidontova, E. E. & Lodge, T. P. (2002) The order–disorder transition and the disordered micelle regime for poly(ethylenepropylene-b-dimethylsiloxane) spheres. *Macromolecules* **35**(26), 9687–9697.
[45] Ward, M. J. (2001) Metastable dynamics and exponential asymptotics in multi-dimensional domains. *Multiple-Time-Scale Dynamical Systems*, IMA Volumes in Mathematics and its Applications, , Springer, New York, pp. 233–259.
[46] Ward, M. J. & Reyna, L. G. (1995) Internal layers, small eigenvalues, and the sensitivity of metastable motion. *SIAM J. Appl. Math.* **55**(2), 425–445.
[47] Zhang, C.-Z. & Wang, Z.-G (March 2006) Random isotropic structures and possible glass transitions in diblock copolymer melts. *Phys. Rev. E* **73**(3), 031804.